www.springer.com/41230
https://doi.org/10.1007/s41230-025-4265-0

Effect of surface recrystallization on high-temperature tensile properties of a directionally solidified DZ409 Ni-based superalloy

Qiang Yang[1], Ya-zhou Li[1], *Fu Wang[1], Jing Wang[1], Di-chen Li[1], and Jian-tao Wu[2]

1. State Key Laboratory for Manufacturing System Engineering, School of Mechanical Engineering, Xi'an Jiaotong University, Xi'an 710049, China

2. Central Iron & Steel Research Institute, Beijing 100081, China

Abstract: Surface recrystallization (RX) is a typical grain defect observed in directionally solidified (DS) Ni-based superalloys. Most studies have focused on the RX behavior and its impact on the mechanical properties of single-crystal (SC) superalloys, with limited research on its influence on the high-temperature mechanical properties of DS superalloys. This study systematically investigated the effect of RX on the high-temperature tensile properties of a DS DZ409 superalloy. The results show that at 650 °C, the yield strength decreases almost linearly with an increase in RX fraction. A significant reduction in elongation is observed as the RX fraction increases from 0% to 4.9%. However, beyond this point, further increase in RX fraction leads to minimal changes in elongation. At 950 °C, both yield strength and elongation decrease as the RX fraction increases from 0% to 4.9%. At 650 °C, fractures in the RX DS superalloys exhibit a mixed mode of transgranular and intergranular cleavage fracture, while at 950 °C, it features a combination of ductile and intergranular dimple fractures. The failure mechanism of the RX DS superalloy is associated with the introduction of transverse grain boundaries (GBs) during RX. In the early stages of tensile testing at intermediate and high temperatures, cracks can easily initiate at these GBs. Subsequently, the cracks propagate along the GBs into the DS matrix, ultimately leading to failure of the DS superalloy.

Keywords: Ni-based superalloy; directional solidification; recrystallization; intermediate- and high-temperature tensile properties

CLC numbers: TG146.1+5 **Document code:** A **Article ID:** 1672-6421(2025)04-463-08

1 Introduction

Due to the elimination of transverse grain boundaries (GBs) and the alignment of GBs parallel to the main stress axis, directionally solidified (DS) blades and vanes made from Ni-based superalloys exhibit excellent mechanical properties at elevated temperatures. These components are widely used in advanced aircraft engines and heavy industrial gas turbines (IGTs) [1, 2]. Surface recrystallization (RX) is a critical defect in these components, causing by the residual strain. During the heat treatment processes, the residual strain serving as the impetus for the initiation and progression of RX under the promotion of high temperature [3].

As the advanced directional alloys have been developed and blade and vane designs have become increasingly complex, surface RX has emerged as a major defect contributing to high scrap rates of DS components. Researchers generally believe that surface RX can diminish the high-temperature performance of these parts. Nonetheless, research works on the effects of surface RX on the high-temperature mechanical properties of DS blades and vanes are surprisingly limited in the open references. Most studies have focused on the behavior of surface RX in directionally solidified single-crystal (SC) superalloys [4-16], as well as its impact on the room temperature mechanical properties of SC superalloys [17-23], with little research addressing its influence on the high-temperature mechanical properties of DS blades and vanes [24, 25].

***Fu Wang**

Male, born in 1982, Ph. D. His research interest mainly focuses on preparation of single crystal turbine blades and additive manufacturing.

E-mail: fuwang@xjtu.edu.cn

Received: 2024-11-30; Revised: 2025-01-13; Accepted: 2025-01-21

In this study, DS DZ409 superalloy samples underwent sandblasting for varying durations and subsequent heat treatment to induce different depths of surface RX. The influence of surface RX on high-temperature tensile properties at various temperatures was systematically investigated. Additionally, combined with simulation analysis, the fracture modes of the DS superalloy with and without RX at different temperatures were analyzed, revealing the failure mechanisms in the RX DS superalloys.

2 Experimental procedures

DZ409 superalloy with the nominal composition of 12.2 Cr, 0.13 C, 1.4 Mo, 3.93 W, 4.0 Al, 4.06 Ti, 4.5 Ta, 0.088 B, 0.021 Zr, 8.57 Co, 0.48 Hf, and balance Ni, in wt.%, was used as raw material in the present study. As-cast DS hollow dummy blades, as shown in Fig. 1, were solidified using a Bridgeman furnace. The directional solidification processes are as follows: Firstly, melting the alloy in a crucible which was positioned in the induction melting coil. Then, fixed the investment mold cluster onto the chill plate and raised it into the mold-heater. A vacuum of 1×10^{-3} Pa would be achieved in the furnace chamber before preheating the mold. After equalizing the mold temperature of 1,480 °C, the melted alloy with the temperature of 1,490 °C was poured into the mold, and finally the DS hollow dummy blades were obtained under a withdrawal rate of 6 mm·min^{-1}. Then, the specimens for high-temperature tensile testing were cut off from these blades. The specimens contain two columnar grains which have 15±2° and 25±2° misorientation to [001] crystallization orientation tested by Laue method. Their grain boundary (GB) is parallel to the gravity direction (i.e., the tensile direction of in tensile testing).

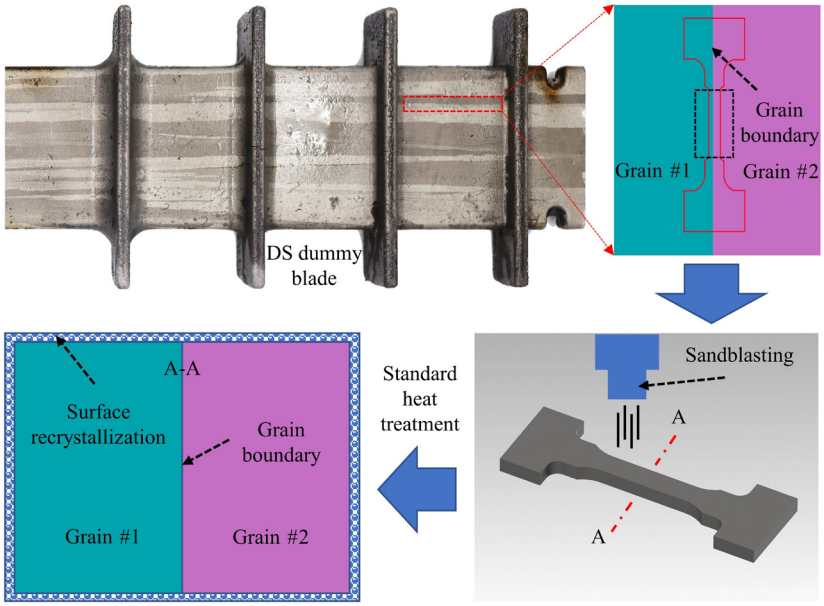

Fig. 1: Preparation of specimens used in high-temperature tensile testing

To induce varying fractions of RX, the gauge lengths of the specimens were subjected to sandblasting using Al_2O_3 sand with a particle size of 60 mesh for 0 s, 15 s, 30 s, and 45 s. The specimens were then subjected to solution treatment (1,180 °C/2 h+1,230 °C/3 h, AC) and aging treatment [(1,080 °C/4 h, AC)+(845 °C/24 h, AC)] in a vacuum furnace. Subsequently, the specimens before tensile testing were transversely cut at the gauge position, and the microstructure was observed using optical microscopy after etching with an etchant composed of 60 mL C_2H_5OH, 40 mL HCl, and 2 g $CuCl_2\cdot2H_2O$. The fraction of surface RX, defined as the ratio of the surface RX area to the cross-sectional area at the gauge position of the specimens, was calculated using Image-Pro Plus software. Three measurements were conducted for each surface RX specimen that underwent various sandblasting durations, which were then used in tensile testing at 650 °C and 950 °C, with a stress loading rate maintained at 0.001 s^{-1}. The fracture surfaces were examined using scanning electron microscopy (SEM, Zeiss Sigma300, Carl Zeiss AG, Oberkochen, Germany).

3 Simulation

To understand the fracture mechanism of the recrystallized specimens, fracture behavior was simulated using ABAQUS software (Abaqus/CAE 2023, Dassault Systèmes, France). To accurately model the material's mechanical behavior and thermal effects, it is crucial to describe the equilibrium state under external forces, which is done using the static equilibrium equation:

$$\nabla\cdot\sigma+f=0 \quad (1)$$

where σ is the stress tensor, and f is the body force density.

The material's deformation behavior is described by constitutive relations. For elastic deformation, the stress-strain relationship follows Hooke's Law:

$$\sigma=\mathrm{C}\cdot\epsilon \quad (2)$$

where σ is the stress tensor, ϵ is the strain tensor, and C is the stiffness matrix, which depends on the material's Young's modulus E and Poisson's ratio ν [7]. In cases of large deformation, plastic deformation may occur, and the yield

criterion is typically followed the Von Mises criterion:

$$\sigma_{eq} = \sqrt{\frac{1}{2}\left(\sigma_{11}^2 + \sigma_{22}^2 + \sigma_{33}^2 - \sigma_{11}\sigma_{22} - \sigma_{22}\sigma_{33} - \sigma_{33}\sigma_{11} + 3\left(\tau_{12}^2 + \tau_{23}^2 + \tau_{31}^2\right)\right)} \quad (3)$$

where σ_{eq} is the equivalent stress, representing the yield behavior of the material [26].

Thermal effects on the material's deformation are significant at high temperatures. Thermal expansion strain ($\sigma_{thermal}$) is given by:

$$\sigma_{thermal} = \alpha\Delta T \quad (4)$$

where α is the material's coefficient of thermal expansion, and ΔT is the temperature change. The change of temperature significantly impacts the strain of material, as well as its elastic modulus and yield strength, thereby altering the material's mechanical properties [27].

To simulate the fracture mechanism of the superalloy, a 10×5 rectangular domain was established. The distribution of surface recrystallization was modeled based on Voronoi cells and the actual observed morphologies of RX layers, with grain boundaries of 0.03 mm wide established on the grain boundaries, dividing the entire rectangle into a layer of recrystallized grains and a large grain. After assigning material parameters, a fixed boundary condition was applied to the left edge, and a displacement was applied to the right edge to induce fracture in the model. Temperature conditions (650 °C/950 °C) were set, and the mesh was discretized into triangular elements with a side length of 0.1 mm. The physical parameters used in the simulation were calculated using Thermal-Calc software, as shown in Fig. 2.

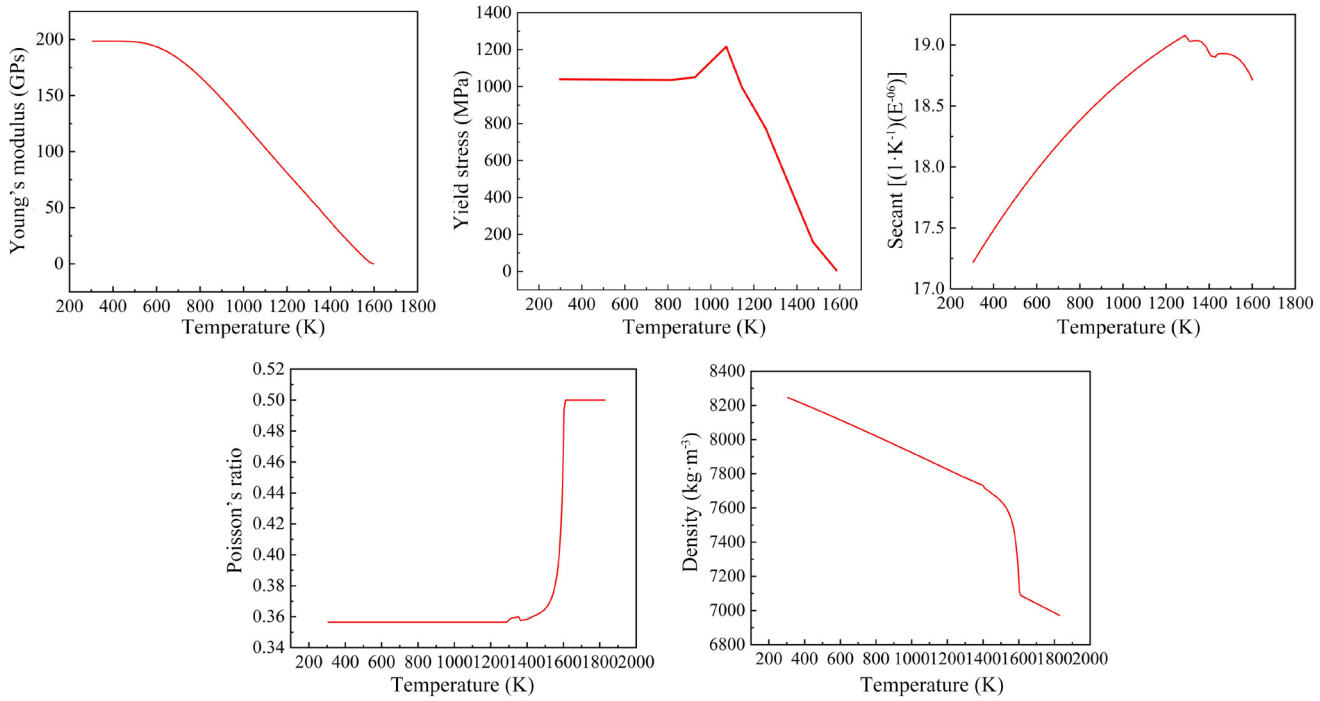

Fig. 2: Physical parameters used in ABAQUS simulation

4 Resutls and discussion

4.1 Morpholgies of surface RX layers before tensile test

Figure 3 illustrates the morphologies of surface RX layers in the cross-sections of specimens underwent sandblasting for varying durations. After 15 s of sandblasting, a thin, discontinuous RX layer composed of fine grains forms, with an average thickness of approximately 17 μm, where the GBs are chaotically arranged. As the sandblasting duration increases to 30 s, the layer gradually becomes thicker and more continuous; most grains grow larger, and their boundaries align more vertically to the matrix. After 45 s, the layer becomes nearly continuous, and the grains grow significantly larger, with an average thickness of about 56 μm, and the GBs are predominantly vertical to the matrix. The fractions of surface RX were measured and calculated to be 4.9%, 6.2%, and 8.2% for the specimens with a sandblasting duration of 15 s, 30 s, and 45 s, respectively. Additionally, a small number of micropores are observed in the DS matrix, and these micropores can accelerate the propagation rate of cracks that originate from the RX layer within the matrix and reduce the mechanical properties of the DS superalloy.

4.2 Influence of surface RX on high-temperature tensile properties at 650 °C and 950 °C

Figure 4 shows the stress-strain curves of specimens with different surface RX fractions, along with their yield strength ($\sigma_{0.2}$) [Fig. 4(a)] and elongation [Fig. 4(b)] at 650 °C. It is evident that an increase in surface RX significantly reduces both yield strength and elongation. As the RX fraction increases, the yield strength decreases almost linearly from approximately 1,171 MPa to about 988 MPa. A notable reduction in elongation is also observed, decreasing from approximately 3.6% to about 0.9% when the RX fraction increases from 0%

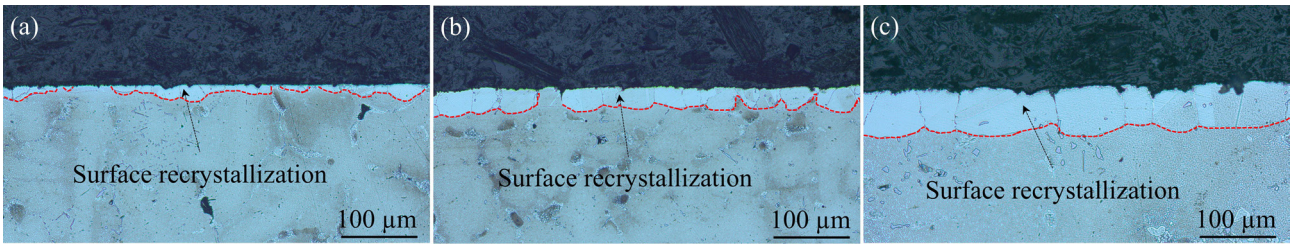

Fig. 3: Morphologies of surface RX layer sandblasted for varying durations: (a) 15 s; (b) 30 s; and (c) 45 s

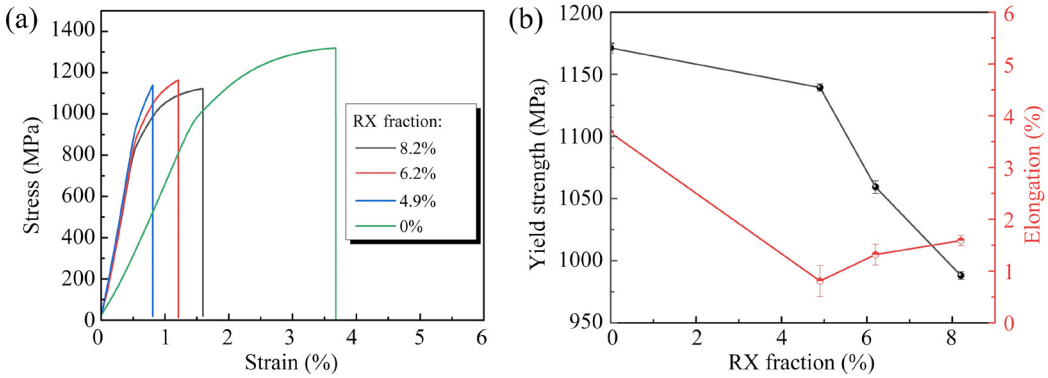

Fig. 4: Influence of RX on high-temperature tensile properties of specimens at 650 °C: (a) stress-strain curves; (b) variation in yield strength and elongation with RX fraction

to 4.9%. Beyond this point, further increases in the RX fraction result in insignificant changes in elongation, indicating that elongation becomes less sensitive to RX fraction increasement beyond this point.

Figure 5 shows the fracture morphologies of specimens with different surface RX fractions at 650 °C. When the RX fraction is 0%, the fracture exhibits features of cleavage steps and river patterns [Figs. 5(a2, a3)], indicating that the fracture mode is transgranular cleavage fracture. For the RX specimens, the internal regions of the fracture display the transgranular cleavage fracture mode with characteristics of cleavage steps and river patterns [Figs. 5(b2, c2, and d2)]. However, in the outer edge areas of these specimens, specifically in the RX regions, the fracture presents a sugar-like pattern with varying degrees of polyhedral grain shapes. This suggests that the fracture mode in these regions is intergranular fracture, as indicated in Figs. 5(b3, c3, and d3). The observed fracture morphologies generally align with the elongation results of the specimens at 650 °C.

Figure 6 illustrates the stress-strain curves of specimens with different surface RX fractions at 950 °C, along with their yield strength ($\sigma_{0.2}$) and elongation. Similar to the results at 650 °C, an increase in surface RX significantly reduces both yield strength and elongation. A significant reduction in yield strength from approximately 625 MPa to about 565 MPa, as well as a decrease in elongation from approximately 6.3% to about 2.8%, is observed when the RX fraction increases from 0% to 4.9%. Beyond this point, further increases in RX fraction lead to insignificant changes in yield strength and elongation, suggesting that neither yield strength nor elongation is significantly affected by RX fraction increasement beyond this point.

Figure 7 shows the fracture morphologies of specimens with different surface RX fractions at 950 °C. When the RX fraction is 0%, the fracture exhibits dimples [Figs. 7(a2, a3)], indicating that the fracture mode is ductile fracture. For the specimens with a RX fraction of 4.9%, 6.2%, and 8.2%, the internal regions of the fracture also show dimples [Figs. 7(b2, c2, and d2)]. In comparison to 650 °C, a brittle-to-ductile transition occurs in the specimens at 950 °C. In the RX regions, the fracture presents characteristics of layered and intergranular dimple fracture, as indicated in Figs. 7(b3, c3, and d3).

The present study indicates that the formation of RX significantly reduces the intermediate- and high-temperature tensile properties of DS superalloys. This reduction can be attributed to crack initiation and propagation caused by the RX during tensile testing. When surface RX occurs, numerous transverse GBs, which are normal to the applied stress, are introduced into the DS superalloy. These GBs become the weakest regions at intermediate and high temperatures. Due to the lower strength of the RX layer and the inhomogeneous deformation between this layer and the DS matrix, cracks can readily initiate at the GBs in the early stages of tensile testing. Subsequently, these cracks propagate along the grain boundaries into the DS matrix, as illustrated in Fig. 8, leading to the failure of the DS specimens. Consequently, the tensile properties of the RX specimens are lower compared to those of RX-free DS specimens. As the testing temperature increases to 950 °C, the strength of the transverse GBs further diminishes compared to that at 650 °C. This results in more rapid crack initiation and propagation in these GBs, as shown in Fig. 8(b). Therefore, the yield strengths of the specimens are significantly reduced at higher temperatures.

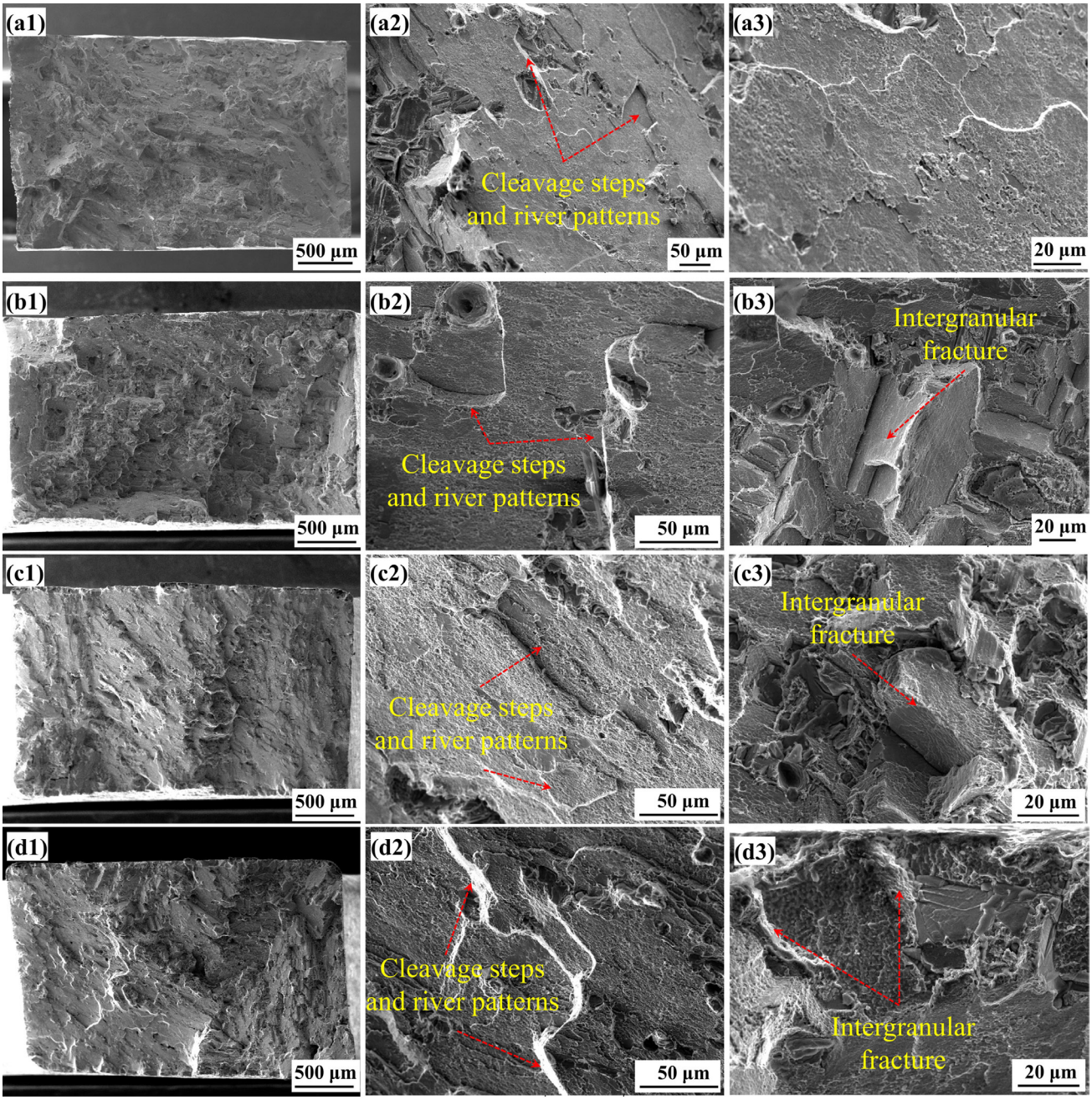

Fig. 5: Fracture morphologies of specimens with different surface RX fractions at 650 °C: (a1–a3) 0%; (b1–b3) 4.9%; (c1–c3) 6.2%; and (d1–d3) 8.2%

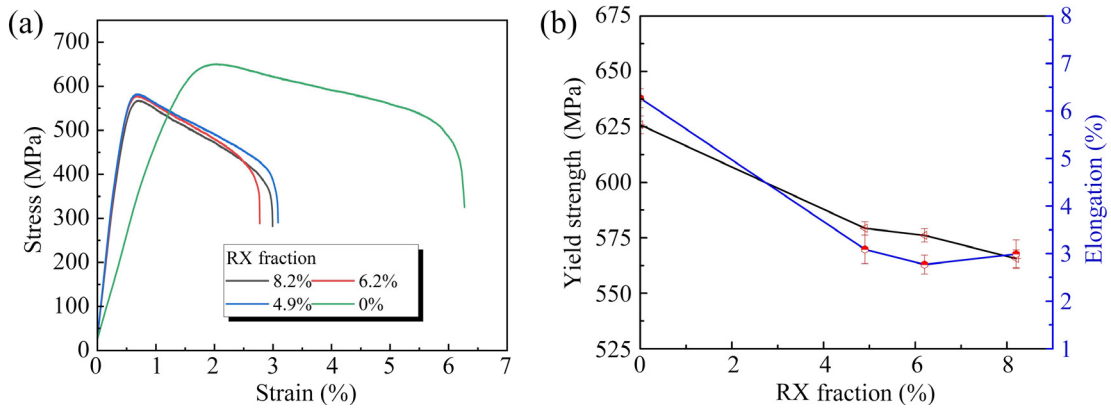

Fig. 6: Influence of RX on high-temperature tensile properties of specimens at 950 °C: (a) stress-strain curves; (b) variation in yield strength and elongation with RX fraction

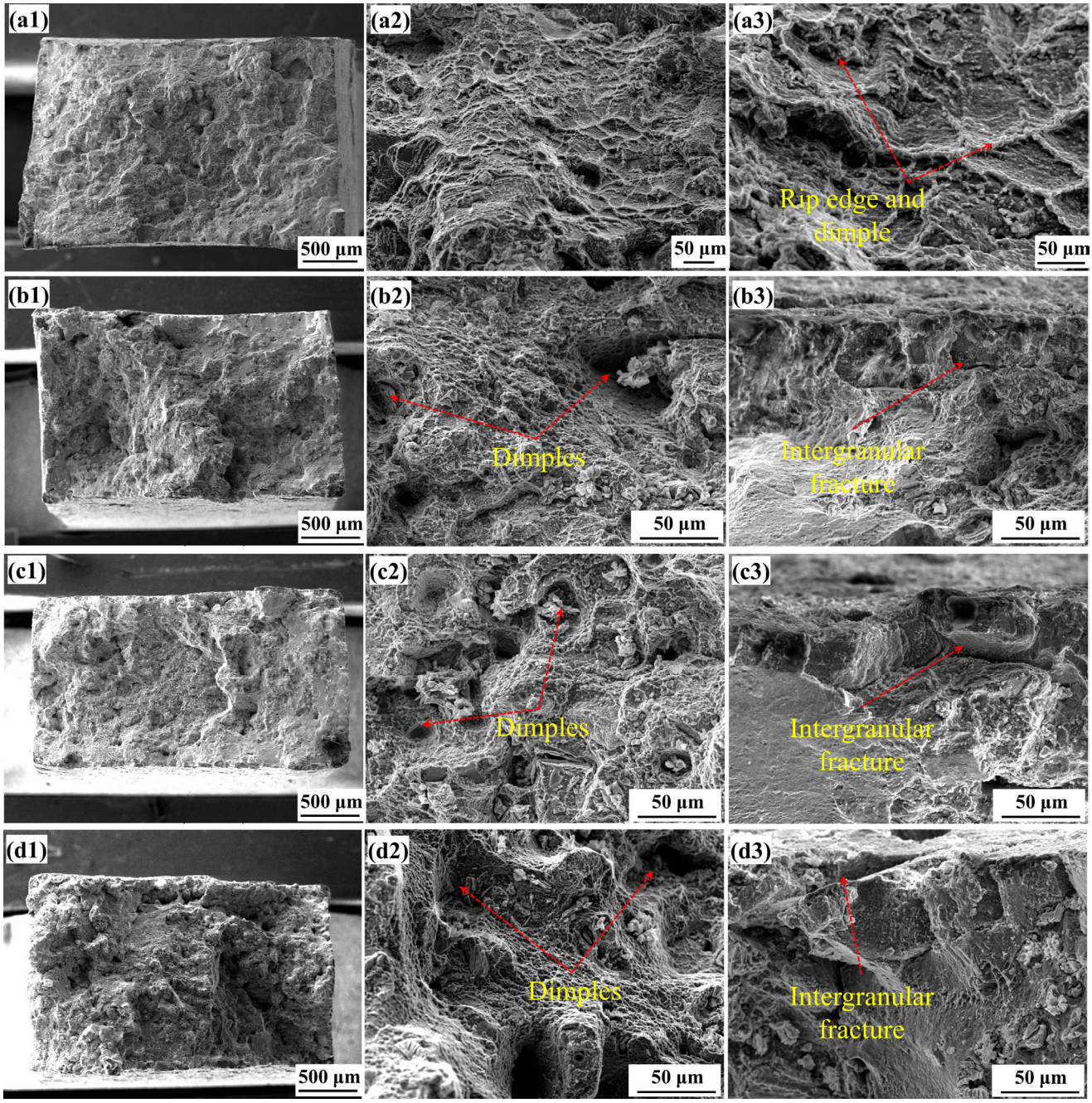

Fig. 7: Fracture morphologies of specimens with different surface RX fractions at 950 °C: (a1–a3) 0%; (b1–b3) 4.9%; (c1–c3) 6.2%; and (d1–d3) 8.2%

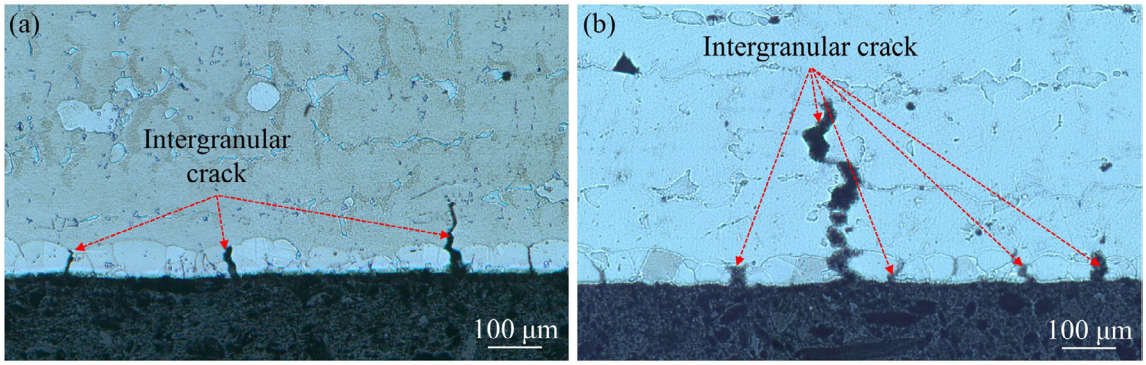

Fig. 8: Longitudinal micrographs of recrystallization specimens (RX fraction: 8.2%) near to fracture surface after tensile testing at different temperatures: (a) 650 °C; and (b) 950 °C

Previous studies [25] suggest that the morphologies of RX GBs significantly influence the mechanical properties of SC superalloys. GBs with a larger deviation angle from the direction of the applied principal stress are more likely to promote crack initiation, and the rate of crack propagation is faster. As shown in Fig. 2, when the RX fraction is low, the number of transverse GBs perpendicular to the main stress axis is minimal. Conversely, when the RX fraction is high, the number of these transverse GBs increases, allowing cracks to initiate and propagate more easily in specimens with a larger RX fraction, ultimately leading to specimen failure. This observation is further supported by the simulation results presented in Fig. 9. With the increase of the RX fraction from 4.9% to 8.2%, the number of transverse GBs perpendicular to the main stress axis increases remarkablely [Figs. 9(a, b)], and the speed and depth of crack propagation sharply increase [Figs. 9(c, d)]. Therefore, as the RX fraction increases, the yield strength of the RX specimens decreases at 650 °C. When the testing temperature is raised to 950 °C, the GBs lose significant strength. Consequently, the influence of GB morphologies becomes less pronounced, and the tensile properties change insignificantly with further increases in RX fractions.

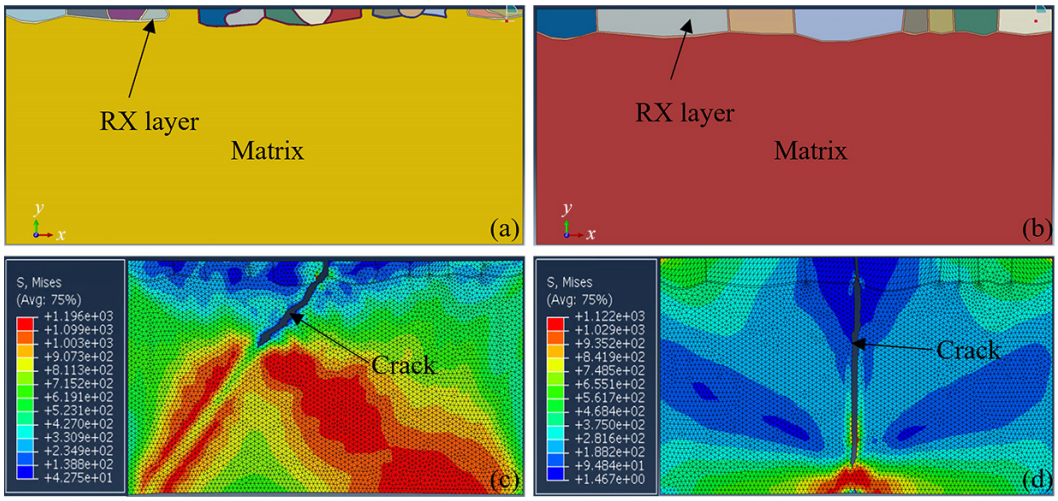

Fig. 9: 2D Voronoi models and simulated crack formation during tensile testing at 650 °C: (a, c) 4.9%; and (b, d) 8.2% RX fraction specimens

5 Conclusions

In this study, the influence of surface recrystallization (RX) on the high-temperature tensile properties of directionally solidified (DS) Ni-based superalloy was investigated. The following conclusions can be drawn:

(1) At 650 °C, as the RX fraction increases, the yield strength decreases almost linearly. A significant reduction in elongation is observed when the RX fraction increases from 0% to 4.9%. However, beyond this point, further increases in the RX fraction result in minimal changes in elongation. At 950 °C, a reduction in both yield strength and elongation occurs when the RX fraction increases from 0% to 4.9%. Beyond this point, further increases in RX fraction lead to negligible changes in both yield strength and elongation.

(2) At 650 °C, when the RX fraction is 0%, the fracture exhibits a transgranular cleavage fracture mode. For RX specimens, the internal regions of the fracture maintain this transgranular cleavage mode, but in the RX regions, the fracture transitions to an intergranular fracture mode. At 950 °C, when the RX fraction is 0%, the fracture shows ductile fracture characteristics. For RX specimens, the internal regions of the fracture also display ductile fracture, while the RX regions exhibit intergranular dimple fracture.

(3) When surface RX occurs, a significant number of transverse grain boundaries (GBs), oriented normal to the applied stress, are introduced into the DS superalloy. These GBs become the weakest regions at intermediate and high temperatures. During the early stages of tensile testing, cracks can easily initiate at these GBs. Subsequently, these cracks propagate along the GBs into the DS matrix, ultimately leading to the failure of the DS superalloy.

Acknowledgments

The work is financially supported by the National Science and Technology Major Project (No. HT-J2019-VI-0020-0136), the National Youth Talent Support Program, and the Fundamental Research Funds for the Central Universities (No. xtr072024004).

Conflict of interest

The authors declare that they have no known competing financial interests or personal relationships that could have appeared to influence the work reported in this paper.

References

[1] Reed R C. The superalloys: Fundamentals and applications. Cambridge University Press, New York, 2006.

[2] Wang H, Zhang X, Meng J, et al. A new model of competitive grain growth dominated by the solute field of the nickel-based superalloys during directional solidification. J. Alloy. Compd., 2021, 873: 159794.
[3] He Y, Hou X, Tao C, et al. Recrystallization and fatigue fracture of single crystal turbine blades. Eng. Fail. Anal., 2011, 18: 944–949.
[4] Rettberg L, Pollock T. Localized recrystallization during creep in nickel-based superalloys GTD444 and René N5. Acta Mater., 2014, 73: 287–297.
[5] Liu Y X, Lin Y C, Li H B, et al. Study of dynamic recrystallization in a Ni-based superalloy by experiments and cellular automaton model. Mater. Sci. Eng. A, 2015, 626: 432–440.
[6] Panwisawas C, Mathur H, Gebelin J, et al. Prediction of recrystallization in investment cast single-crystal superalloys. Acta Mater., 2013, 61: 51–66.
[7] Li Z, Xu Q, Liu B. Experimental investigation on recrystallization mechanism of a Ni-base single crystal superalloy. J. Alloy. Compd., 2016, 672: 457–69.
[8] Xiong W, Huang Z, Xie G, et al. The effect of deformation temperature on recrystallization in a Ni-based single crystal superalloys. Mater. Des., 2022, 222: 111042.
[9] Qin L, Pei Y, Li S, et al. Effect of thermal stability of γ′ phase on the recrystallization behaviors of Ni-based single crystal superalloys. Mater. Des., 2017, 130: 69–82.
[10] Tian L, Xu C, Ma C. Recrystallization of a single crystal Ni-base superalloy in <011> and <111> orientations. Mater. Charact., 2017, 127: 116–120.
[11] Xiao Q, Xu Y, Liu X, et al. Oxidation-induced recrystallization and damage mechanism of a Ni-based single-crystal superalloy during creep. Mater. Charact., 2023, 195: 112465.
[12] Li Y, Tao C, Zhang W. Dynamic recrystallization behavior of a directionally solidified superalloy. Adv. Eng. Mater., 2007, 9: 867–871.
[13] Mathur H, Panwisawas C, Jones C. Nucleation of recrystallisation in castings of single crystal Ni-based superalloys. Acta Mater., 2017, 129: 112–123.
[14] Xu Y, Gong Y, Zhang W, et al. Microstructure evolution and dynamic recrystallization mechanism induced by grinding of Ni-based single crystal superalloy. J. Mater. Process. Tech., 2022, 310: 117784.
[15] Li Z, Xiong J, Xu Q, et al. Deformation and recrystallization of single crystal nickel-based superalloys during investment casting. J. Mater. Process. Tech., 2015, 217: 1–12.
[16] Li Y, Zhou H, Li L, et al. Recrystallization in a Ni-based single-crystal superalloy traced by quasi-in-situ EBSD. Scripta Mater., 2025, 255: 116369.
[17] Zhang B, Lu X, Liu D, et al. Influence of recrystallization on high-temperature stress rupture property and fracture behavior of single crystal superalloy. Mater. Sci. Eng. A, 2012, 551: 149–153.
[18] Meng J, Jin T, Sun X, et al. Effect of surface recrystallization on the creep rupture properties of a nickel-base single crystal superalloy. Mater. Sci. Eng. A, 2010, 527: 6119–6122.
[19] Zhang B, Liu C, Lu X, et al. Effect of surface recrystallization on the creep rupture property of a single-crystal superalloy. Rare Metal., 2010, 29: 413–416.
[20] Jo C, Kim H. Effect of recrystallisation on microstructural evolution and mechanical properties of single crystal nickel based superalloy CMSX-2 Part 2-Creep behaviour of surface recrystallised single crystal. Mater. Sci. Tech., 2003, 19: 1671–1676.
[21] Ma X, Jiang J, Zhang W, et al. Effect of local recrystallized grains on the low cycle fatigue behavior of a nickel-based single crystal superalloy. Crystals, 2019, 9: 312.
[22] Ma X, Shi H, Gu J, et al. Influence of surface recrystallization on the low cycle fatigue behaviourof a single crystal superalloy. Fatigue Fract. Eng. Mater. Struc., 2015, 38: 340–51.
[23] Shi Z, Liu S, Yue X, at al. Effect of cellular recrystallization on tensile properties of a nickel-based single crystal superalloy containing Re and Ru. J. Iron. Steel. Res. Int., 2017, 24: 1059–1064.
[24] Xie G, Wang L, Zhang J, et al. Influence of recrystallization on the high-temperature properties of a directionally solidified Ni-base superalloy. Metall. Mater. Trans. A, 2008, 39: 206–210.
[25] Xie G, Lou L H. Influence of the characteristic of recrystallization grain boundary on the formation of creep cracks in a directionally solidified Ni-base superalloy. Mater. Sci. Eng. A, 2012, 532: 579–584.
[26] Zhang Y, Zhang X Z, Wang J, et al. High cycle fatigue life prediction model based on crystal plasticity and continuum damage mechanics for Ni-based single crystal superalloys under a multiaxial stress state. Int. J. Plast., 2023, 162: 103526.
[27] Wang Z J, Grosseau-Poussard J C, Panicaud B, et al. Finite element analysis of stress evolution during the high temperature oxidation of Ni30Cr+Cr_2O_3 systems. J. Alloy. Compd., 2022, 904: 164094.